

Visualizing Tensor Fields in Geomechanics

Alisa Neeman*

Computer Science Department,
UCSC

Boris Jeremic†

Department of Civil and Environmental Engineering,
UC Davis

Alex Pang‡

Computer Science Department,
UCSC

The study of stress and strains in soils and structures (solids) help us gain a better understanding of events such as failure of bridges, dams and buildings, or accumulated stresses and strains in geological subduction zones that could trigger earthquakes and subsequently tsunamis. In such domains, the key feature of interest is the location and orientation of maximal shearing planes. This paper describes a method that highlights this feature in stress tensor fields. It uses a plane-in-a-box glyph which provides a global perspective of shearing planes based on local analysis of tensors. The analysis can be performed over the entire domain, or the user can interactively specify where to introduce these glyphs. Alternatively, they can also be placed depending on the threshold level of several physical relevant parameters such as double couple and compensated linear vector dipole. Both methods are tested on stress tensor fields from geomechanics.

CR Categories: I.3.6 [Computer Graphics]: Methodology and Techniques—Interaction Techniques;

Keywords: symmetric tensors, stress tensor, seismic moment tensor, anisotropic, deviatoric, double couple, compensated linear vector dipole

1 INTRODUCTION

One of the important tensors of interest in geomechanics are stress tensors. These are second order symmetric tensors with six independent values. While there are a few techniques already available for visualizing symmetric tensor fields, not every tensor visualization technique is suitable or helpful for every type of tensor and its domain of use. Thus, we first explore the tensor types, their domains, the qualities and features of interest, and commonalities and differences in the analysis and visualization techniques.

Based on our study, we report on our efforts to address a need in seismology and geomechanics. Both disciplines try to discover where the earth or material will fracture and shift, or describe such an event that has occurred. Towards this end, we treat geomechanical stress tensors as seismic or acoustic moment tensors, using standard analysis to find features that suggest cracking, shear fracture or earth flow. Moment tensor analysis provides scalar quantities that describe these stress features at each sample point. We introduce a simple plane-in-a-box glyph, to illustrate the plane of causative forces. Just as 2D vector fields can be visualized with arrow glyphs, plane-in-a-box glyphs seem to be a natural extension for visualizing the next higher order tensor in 3D. A plane in a 3D volume portrays two out of the

three orthogonal eigenvectors in a symmetric stress tensor, while the normal to the plane implies the third. The plane is spanned by the major and medium eigenvectors based on their absolute eigenvalues. Depending on the seismic feature in a moment tensor, this can indicate the direction of cracking, particle motion, or simply the causative forces. In seismology, the fault plane will lie roughly 45 degrees off from the planes of major stress. It also provides a glyph that will indicate directions in line with a standard tensor ellipsoid. The orientation of the plane will be very similar to a stress glyph with high planar isotropy. A stress glyph with high linear anisotropy would be like a line on the plane glyph. Thus, an idea similar to the plane-in-a-box glyph is the use of flat, planar but transparent disks which are then volume rendered [25]. However, our technique is not only much cheaper, but highly interactive. It also shows global trends such as regions where stresses lie neatly in parallel lines or clusters of noisy chaos.

When using glyphs for visualization, a main concern is clutter and occlusion. Occlusion is view dependent and occurs when foreground objects, small or large, obscure background objects. Clutter, on the other hand, is the general sense of disorder. Compared to tensor ellipsoids, tensor boxes, or superquadric tensor glyphs [17] the plane-in-a-box glyphs are much simpler and do not show the relative magnitudes of the eigenvalues. Instead, they simply show the orientation of the two eigenvectors associated with the absolute values of the two largest eigenvalues. This is sufficient in showing the important aspects of geomechanical stress tensors and because the glyphs do not take up as much volume, they also help reduce occlusion and clutter. The planes themselves can also be scaled so that they only span half (or less) of the distance to their nearest neighbors. In this way, we further reduce the amount of occlusion in the images. Furthermore, we allow the user to set feature-based thresholding constraints for each feature (and invert them as well). Finally, we provide user-defined feature-based opacity functions. Scaled glyphs which show magnitude are less important since such scalar features can be illustrated and highlighted through color, opacity and thresholding.

2 SECOND ORDER SYMMETRIC TENSOR

In preview, we briefly review second order symmetric tensors used to represent stress. Second order symmetric tensors are described mathematically using a 3x3 matrix where the off diagonal components are equal so $s_{ij} = s_{ji}, i \neq j$ as follows:

$$S = \begin{bmatrix} s_{11} & s_{12} & s_{13} \\ s_{12} & s_{22} & s_{23} \\ s_{13} & s_{23} & s_{33} \end{bmatrix} \quad (1)$$

In a stress tensor, the three diagonal components represent normal stress, and the off diagonal elements comprise shear stresses.

*e-mail: aneeman@cse.ucsc.edu

†e-mail:jeremic@ucdavis.edu

‡e-mail:pang@cse.ucsc.edu

A symmetric tensor S can be decomposed into two matrices M and T such that $S = TMT^T$, where T is the column ordered matrix of orthogonal eigenvectors, and M is the diagonal matrix with eigenvalues corresponding to the eigenvectors in the columns of T .

Since the symmetric tensor is assumed to lie on cartesian coordinates, the interpretation of T is the transformation needed to reorient S such the shear components are zero. Note that for stress tensors, the eigenvalues can be both positive and negative. Positive eigenvalues indicate compression while negative eigenvalues indicate tensile forces.

Concrete structures can withstand large amounts of compression, but are very weak under tensile forcing. Likewise, in soils, places where there are large changes from tensile to compressive forces may indicate potential cracks and fault lines. More quantitative measures that are of primary interest to geomechanics are described in Section 3.

3 STRESS TENSORS IN VARIOUS DOMAINS

This paper focuses on visualization techniques for second order symmetric tensors representing stress in soils and structures. Since symmetric tensors can represent a plethora of physical phenomena, it is reasonable to ask whether the techniques from one domain are applicable to stress tensors from other domains as well.

3.1 Fluid Stress Tensors

Fluid flow research encompasses a whole range of disciplines from ocean circulation and weather forecasting to aeronautics. Analysis includes examining the velocity gradient tensor, which can in turn be decomposed into a rotational tensor and a rate of strain tensor. Another important quantity is the stress tensor which measures how a fluid element may deform under stress. The fluid stress tensor can be decomposed into a pressure term P leading to a change in volume but not in shape, and a deviatoric tensor τ which produces a change in shape.

The fluid stress tensor is a symmetric second order tensor which can be visualized using a number of techniques. Typically, either the absolute values of the eigenvalues are first sorted such that $|\lambda_3| \geq |\lambda_2| \geq |\lambda_1|$, or the signed eigenvalues are sorted such that $\lambda_3 \geq \lambda_2 \geq \lambda_1$. That is, the tensor field is separated into three orthogonal vector fields corresponding to each of the sorted eigenvalues. One related feature measure is the eigen difference [27]. It is a scalar K defined as:

$$K = 2\lambda_2 - (\lambda_1 + \lambda_3) \quad (2)$$

where K is a positive value for planar degenerate tensors (identical major and medium eigenvectors), and a negative value for linear degenerate tensors (identical medium and minor eigenvectors). We used this quantity for glyph color and drawing constraints.

A popular method to visualize second order tensors is with hyperstreamlines [6]. While this technique is a very intuitive extension of streamlines to eigenvector fields and provides a continuous representation of the eigenvector fields, it does have some drawbacks. First, because of the visual clutter and occlusion, typically only one eigenvector field is visualized at a time thereby only providing a partial representation of the tensor field. Secondly, it is generally impossible to sort the eigenvalues in a consistent and continuous fashion [27] and hence the hyperstreamlines, while continuous, may exhibit sudden changes in directions.

Another way of visualizing these tensors is with glyphs that are placed at discrete locations in the field. There are a number of glyphs that have been designed to date. A recent study by Hashash et al. [10] evaluated several glyphs in their ability to show certain physical properties. Among the glyphs included in the study are: (i) Lamé stress ellipsoid which is a glyph where its three axes are defined by the absolute magnitudes of the principal stresses; (ii) Haber glyph which consists of a cylindrical rod through an elliptical disk. The half length of the rod represents the magnitude of the major principal stress, while the shape of the disk is controlled by the magnitudes of the median and minor stresses; (iii) Cauchy's stress quadric glyph which uses the tensor components in a quadric surface equation such that the glyph is oriented in the principal directions; and (iv) Reynolds stress glyph which is defined such that the distance from the origin of the glyph to any point on its surface is the magnitude of normal stress in that direction. This glyph is used to gain insights from turbulence and stress measurements in 3D flows.

Aside from the consideration of what physical properties are encoded in the design of these glyphs, a common trait among their usage is the question of scale and position. That is, how large should the glyphs be, and how dense and where should they be placed. The glyph placement is of itself a research problem [24]. In this paper, we use a combination of transparency, user interaction, and filtering by the physical properties to place and render our plane-in-a-box glyphs.

3.2 Diffusion MRI Tensors

Diffusion Tensor Magnetic Resonance Imaging (DT-MRI) describe diffusion of water molecules through tissue. According to Kindlmann and Weinstein [18], the key feature of interest is the anisotropic motion of water molecules. They note that with brain scans, doctors wish to visualize white matter, the fibrous structure which connects major regions of the brain. Westin, et al. decomposed MRI diffusion tensors and correlated *linear anisotropy* with the major white matter tracts [26]. An important difference between the diffusion tensors and the fluid stress tensors is that the diffusion tensors are positive definite with positive eigenvalues.

A diffusion tensor is classified as being isotropic where $\lambda_1 \simeq \lambda_2 \simeq \lambda_3$, planar anisotropic where $\lambda_1 \simeq \lambda_2 \geq \lambda_3$, or linear anisotropic where $\lambda_1 \geq \lambda_2 \simeq \lambda_3$. The degree of each case is determined as follows:

$$\frac{\lambda_1 - \lambda_2}{\lambda_1 + \lambda_2 + \lambda_3} \quad \frac{2(\lambda_2 - \lambda_3)}{\lambda_1 + \lambda_2 + \lambda_3} \quad \frac{3\lambda_3}{\lambda_1 + \lambda_2 + \lambda_3}$$

(linear case) (planar case) (isotropic case)

A key difference between diffusion tensors and fluid stress tensors is that diffusion tensors are used to reconstruct the white matter structures which are characterized by chains of tensors with high linear anisotropy. On the other hand, fluid stress tensors are used to learn about the local deformation and volume change of a fluid element. Similarly, geomechanics stress tensors are quite similar to fluid stress tensors minus turbulence. As such, the focus of stress tensors is on shearing deformations of the tensors. Hence, the visualization techniques developed for DT-MRI such as tractography and fiber tracking, volume rendering [18], or glyphs [20, 17] may not be the best methods to visualize geomechanics stress tensors.

3.3 Stresses in Geomaterial Solid

Geomechanics uses stress tensors to understand the behavior of soil and objects embedded in the soil as support for structural elements above (i.e. concrete piles for supporting buildings, bridges, tanks...). Features of interest are, for example, zones with positive stress in piles (tension resulting in cracking of concrete) and zones with large shear stresses in soil (shear failure). Concrete and soils can withstand large compressive forces but fail under tension or in shear (i.e. [13, 14, 11, 15]). Critical features of stress tensor in solids made of geomaterials are zones of sign changes (switch from compressive to tensile behavior resulting in tensile failure) and zones of large shear stresses (resulting in shear failure and possible large shear deformations). Both critical features are usually present close to the (stiff, concrete) pile – (soft surrounding) soil, but can happen anywhere in the solid.

Earlier work on visualizing stresses in geomaterial solid explored the use of hedgehog glyphs, hyperstreamlines and hyperstreamsheets for exploring data sets [12]. Hedgehogs were found inadequate to easily understand the contents of the tensor field. Hyperstreamlines and hyperstreamsheets were more powerful but required separate visuals for each of the three principal stresses.

3.4 Seismic Moment Tensors

Dreger et al. state that the seismic moment tensor M_{ij} provides a general representation of the seismic source [7]. Seismic moment tensors are a variety of stress tensor for an elastic substance, similar to stress tensors for geomechanics. However, they differ in a couple of very important ways.

Seismic moment tensors or acoustic emission moment tensors are created from a measured event such as an earthquake or cracking material. Sound waves are emitted at the event and can be measured. Thus, one major difference is that moment tensors represent a strictly *elastodynamic* source [16]. Second, in geomechanics, a stress tensor relates to forces applied on the exterior surface of a volume. Moment tensors instead relate to forces that cause displacement across an *internal* surface, where the internal surface represents a buried fault [1].

Dreger et al. note that M_{ij} is commonly decomposed into isotropic, double couple (DC) and compensated linear vector dipole (CLVD) components, where each of the components of the moment tensor decomposition is represented as a percentage of the total [7, 19, 16].

3.4.1 Isotropic and Deviatoric Components

A diagonalized moment tensor can be further decomposed into isotropic and deviatoric components. A purely isotropic tensor is characterized by three equal eigenvalues. The isotropy in a moment tensor represents a change in volume. Pure isotropy in a moment tensor is comparable to an ideal explosion (positive eigenvalues) or implosion (negative eigenvalues) [8].

The isotropic portion of both general and moment stress tensors is the identity matrix scaled by the mean of the three eigenvalues. The deviatoric component is the remainder of the original matrix after the isotropic component has been removed.

Below is the mathematical notation for the isotropic and deviatoric components of matrix M , where the trace (tr) is the sum of the diagonal elements and m_i^* is $m_{ii} - tr(M)/3$.

Note that the convention in this field differs from that of DT-MRI tensors. Here, m_1^* has the smallest absolute magnitude and m_3^* the largest.

$$M = \begin{bmatrix} \frac{tr(M)}{3} & 0 & 0 \\ 0 & \frac{tr(M)}{3} & 0 \\ 0 & 0 & \frac{tr(M)}{3} \end{bmatrix} + \begin{bmatrix} m_1^* & 0 & 0 \\ 0 & m_2^* & 0 \\ 0 & 0 & m_3^* \end{bmatrix} \quad (3)$$

In moment tensors, the isotropic portion represents a change in volume. Fluid mechanics uses the additive inverse, $-tr(M)/3$, to represent pressure in a fluid at rest, which may or may not lead to a change in volume depending on whether the fluid is compressible or not. Both differ in usage to the DT-MRI interpretation of isotropy as a geometric shape parameter.

3.4.2 Two Vector Dipoles

Moment tensor elements represent dipoles. A dipole is composed of two equal and opposite vectors laying along an axis orthogonal to both of them. The physical meaning is the direction and angle of earth movement along opposite sides of a fault.

According to Dreger *double couple* (DC) consists of two linear vector dipoles of equal magnitude but opposite sign, resolving shear motion on faults oriented 45 degrees to the principal eigenvectors of M_{ij} [7].

Compensated linear vector dipole (CLVD) refers to when “a change in volume is compensated by particle motion in the plane parallel to the largest stress” [8]. This may be a mechanism for deep earthquakes [19]. CLVD is modeled by eigenvalues proportional to 2, -1, -1, reflecting particle motion. Figure 1 shows the failure mechanisms associated with pure isotropy, DC, and CLVD.

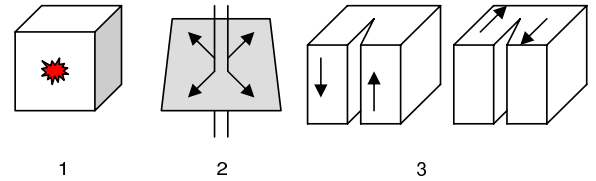


Figure 1: Failure modes for moment tensors. (1) Implosion or explosion, (2) CLVD, (3) DC types.

The contribution of DC and CLVD to the deviatoric component of a moment tensor can be calculated as follows: For components of the diagonalized moment tensor sans isotropy, m_1^* , m_2^* , m_3^* such that

$$|m_3^*| \geq |m_2^*| \geq |m_1^*| \quad (4)$$

$$F = -\frac{|m_1^*|}{|m_3^*|} \quad (5)$$

Note that F is the ratio of the smallest to largest absolutes of the eigenvalues and we expect a value of 0.0 for pure DC and 0.5 for pure CLVD. Assuming the deviatoric is a result of only these two mechanisms,

$$m_{deviatoric} = m_3^*(1 - 2F) \begin{bmatrix} 0 & 0 & 0 \\ 0 & -1 & 0 \\ 0 & 0 & 1 \end{bmatrix} + m_3^*F \begin{bmatrix} -1 & 0 & 0 \\ 0 & -1 & 0 \\ 0 & 0 & 2 \end{bmatrix} \quad (6)$$

For scalar features there are two quantities:

$$DC = m_3^*(1 - 2F) \quad (7)$$

$$CLVD = m_3^*F \quad (8)$$

Following Anderson and Finck [2, 8], percentage of deviatoric that is CLVD can be calculated:

$$\frac{2m_3^*F}{|2m_3^*F| + |m_3^*(1 - 2F)|} \quad (9)$$

The CLVD is doubled so there can be a range of 0.0 – 1.0 instead of 0.0 – 0.5. We use the percentile for culling and coloring glyphs rather than values m_3^*F and $m_3^*(1 - 2F)$ for simplicity.

At present, seismic events are visualized with just a few discrete glyphs. One or two beach balls describe the strike planes and focal mechanism of a seismic event. Similarly, civil engineers currently use a single glyph for each acoustic emission caused by cracking [23]. These glyphs represent point sources where sound waves are emitted due to fracture. In our application, we investigate the use of this decomposition at all points in a volume of stress tensors. We can only experiment in this way because we have a simulation of the entire stress field. With measured data, stress can only be detected at points emitting sound. In other words, when an earthquake occurs, multiple seismometers can pinpoint the sound wave source and a representative moment tensor can be deduced. However, stress anywhere other than the point source of acoustic emission is unknown.

4 GEOMECHANICS DATA

4.1 Data Meaning

Tensor fields resulting from geomechanics computations are mostly related to the state of stress (s_{ij}) and strain (ϵ_{ij}). Of particular importance are the stress tensors as they are mostly used as failure indicators. A large majority of geomechanics theories dealing with inelastic behavior and failure of solids are based in stress space, thus putting a strong emphasis on good understanding of the stress tensor field. Stress tensor fields play a very important role in both static and dynamic simulations. Both types of simulations also result in large, multiple stress tensor data sets. Static simulations will generate stress tensor fields for each incremental step. Loads are applied in a series of increments starting with the self weight of the material followed by the applied forces. In dynamics, the data sets are created for each time step of the simulation.

The geomaterials belong to the so called group of materials with memory. In materials with memory, the response at any iteration of time instance is a function of all the previous responses (behavior). The response is usually measured through the stress field, which means that appropriate visualization tools are very important for understanding the actual behavior of the solid or structure in question. The particular data sets used in this paper are related to two applied geomechanics problems. The first data set represents a finite sized model with two point loads on top, the so called Boussinesq problem (i.e. [21]). The problem is simple enough that the results are known in advance and represents an excellent verification procedure. In addition, a number of symmetry planes available in the model can be used for verification of numerical and visualization procedures. The second data set is from a dynamic (seismic) bridge simulations. It represents a stress field from one time step of an

inelastic, dynamic simulation of a soil–foundation–structure (SFS) bridge system [4, 3]. This data set involves large ratios of stresses between stiff concrete in piles, columns and the main structure and the soft soil beneath. In addition to that, the main characteristics of the stress fields are not known in advance as we use simulations to gain a better understanding of the behavior of the SFS system and the interactions of its components during seismic events.

4.2 Data Representation

The volume of the bridge–soil system is built from finite elements. Each element has a hull of vertex *nodes* that may be shared with neighboring elements. The shape of an element need not be rectilinear. Within each element are *gauss points*. That is, the gaussian method is used to locate points that produce the most accurate integration.

As the simulation progresses, nodes move, inducing stress at the gauss points. Hence, the stress tensor field consists of the induced stresses at these gauss points.

5 IMPLEMENTATION

5.1 Plane-in-a-box Glyph

The plane-in-a-box glyph is quite similar to the tensor ellipsoids for the case when there is strong planar anisotropy. We opted for this simpler glyph since we are primarily interested in regions characterized by high shear. In moment tensors they are characterized by two large eigenvalues and a much smaller minor eigenvalue, and we hypothesize that this is also the case for geomechanical stress. Thus, mapping the tensors to planar glyphs is quite natural. The plane contains the two larger eigenvectors, and the plane normal implies the minor eigenvector direction. The plane itself can also be colored according to other scalar parameters of interest. This glyph presents the same amount of relevant information using a simpler representation. Occlusion can also be reduced by scaling the planar glyphs while maintaining the general orientation of the plane.

The idea of plane-in-a-box is to create a plane with limited extent at each sample point. The size of the planar glyph is limited by a box whose edges are half the distance to each of the neighboring points. If the point is on a face of the volume, we simply extend it out a distance to half the distance of the neighboring interior point.

The plane-in-a-box glyph has two requirements. First, the sampled points must lay on a mesh, preferably a grid (although the grid need not be regular). In either case some connectivity among sample points is necessary. For rectilinear data, we simply sort the points by the Z, Y, and X axes during preprocessing. Once the points are read in, we can deduce connectivity of neighboring points by checking the next and previous row, column and slice.

We soon came to realize that finite element results need not lie on straight lines. For these data sets we take advantage of whatever regularity exists (in our case slices on the Z plane were regular distances apart) and run Delaunay triangulation on the remainder to get connectivity. For both cases, connectivity is stored in an adjacency list.

5.1.1 Creating the Box and Finding Edge-Plane Intersections

The first step in creating glyphs is to create the box whose edges will limit the plane. By iterating through the linked list of rectilinear neighbors, we can determine the minimum

and maximum X, Y, and Z distances to neighbors. We halve them and can even reduce the scale of the distance, if desired. For Delaunay neighbors we use a slightly simpler technique. We check the distance to each neighbor and select the one that is closest. We halve the distance and set that as the bounding distance along axes for which we have no rectilinear distances. This gives us good guarantees against polygon overlap although it may not be proportional to distance between points in all three directions.

Once we have the distances we set the corners of the box using a lookup table which matches minimum or maximum X, Y, and Z to each box corner.

The next step is to create the plane, finding which edges of the box it intersects and where on the edge the intersection occurs. We have a plane defined using point-normal form, where the normal is the eigenvector corresponding to the minor eigenvalue. We convert it to general form

$$Ax + By + Cz + D = 0 \quad (10)$$

where A, B, and C are the X, Y, and Z components of the normal respectively. With the sample point at x_0, y_0, z_0 ,

$$D = (-1 * norm[X] * x_0) - (norm[Y] * y_0) - (norm[Z] * z_0) \quad (11)$$

Then, for each edge of the box, we use Bourke's algorithm [5] to find the intersection by extending the edge until it touches the plane.

$$P_{intersect} = t(P_2 - P_1) \quad (12)$$

where P_1 and P_2 are the points forming an edge of the box. Substituting $t(P_2 - P_1)$ into our implicit plane equation yields

$$A(x_1 + t(x_2 - x_1)) + B(y_1 + t(y_2 - y_1)) + C(z_1 + t(z_2 - z_1)) + D = 0 \quad (13)$$

and solving for t gives

$$t = \frac{Ax_1 + By_1 + Cz_1 + D}{A(x_1 - x_2) + B(y_1 - y_2) + C(z_1 - z_2)} \quad (14)$$

and the intersection occurs at $P_1 + t(P_2 - P_1)$. Once we have an intersection, if it lies on the edge between P_1 and P_2 we update the box's edge index and store the intersection point in its marching cubes array.

In summary, we begin by creating a box which is limited by half the distance its neighbors. We calculate A, B, C and D for our plane, based on the point location and its normal. Then we check each edge of the box to see if the plane intersects it, saving the intersection point and building an edge intersection case index. Finally, the edge intersection index is cross-referenced to a marching cubes index.

5.1.2 Marching Cubes for Simple Planes on an Irregular Grid

After extracting the intersections of the planes with the edges of the cell containing the tensor, the next step is the creation of the triangles that make up the plane. Our algorithm uses a variation on the well-known Marching Cubes [22]. Our algorithm differs in two ways:

- The index is built on edge intersections rather than above/below an isovalue.

- The box is composed of variable-sized quadrilaterals rather than a cube.

We deal with the first item by creating a mapping from each of the 256 marching cubes case indices to its corresponding edge index and save them in our reverse lookup table. More specifically, we iterate through each marching cubes triangle case array, building an active edge index. We then made a hash table with the edge index as the key and the marching cubes index as the value, for fast retrieval. The hash table is used just before the call to marching cubes.

Despite our box forming hexahedron instead of a regular cube, we have found that marching cubes works quite well. Two facts help us. First, when we form the box around a sample point on the plane we guarantee the box will enclose the plane. Second, because we build the case using a plane that spreads to the limits of the box we never see the ambiguous marching cubes indices. Simply, since we build a continuous surface, we don't see holes.

However, two other types of ambiguous cases can occur. One case is where an edge of the box lies in the plane. For such a plane, there are an infinite number of intersection points for the edge and the plane. Further, three edges will claim intersection for each corner of the edge in the plane. In this case a proper marching cubes index cannot be formed. The second ambiguity is where the plane intersects an edge at a box corner. As with the previous case, three edges will claim intersection for each corner of the edge in the plane. The simple solution is to just shift the box a tiny amount along one axis and recalculate. We found this solution effective; we selected the first of multiple possible case indices, and shifted the box back before building the plane's triangles.

We predicted that we would see just a few different marching cubes cases as the point would sit in the middle of the box. This soon proved wrong as the sample point may lie almost anywhere within a skewed box.

5.2 Filtering with Physical Parameters

With the plane-in-the-box glyph, we can quickly perceive trends such as regions of aligned stresses. However, very little can be seen of the volume interior. It is occluded by planes on the volume border. Moreover, simple planes do not provide information about magnitudes of stresses and related features.

We have provided several different scalar measures to aid exploration of a data set, and filtering mechanisms to home in on areas of interest in the volume. The scalar features are: (i) signed isotropy (with both linear and log scaling), (ii) DC, (iii) CLVD, and (iv) eigen difference [27].

The application has a menu for selecting a feature for coloring the planes and a feature for setting plane opacity.

Since the two features, DC and CLVD, can be expressed as percentiles they are automatically scaled from 0 to 1. For isotropy and eigen difference, we set the zero valued features at 0.5. We scaled cool colors (blue) below, down to 0 for negative values and hot colors (red) for positive values scaled up to 1. Opacity can provide some filtering effect as the lowest values are fully transparent. Medium to high values appear more solid and their geometry is highlighted, similar to volume rendering.

The application also has sliders for selecting a range of values for features. For example, a user can select strictly positive isotropy combined with high CLVD. Such combinations allow users to search for domain-specific indicators. The aforementioned, for example, can signify a crack when

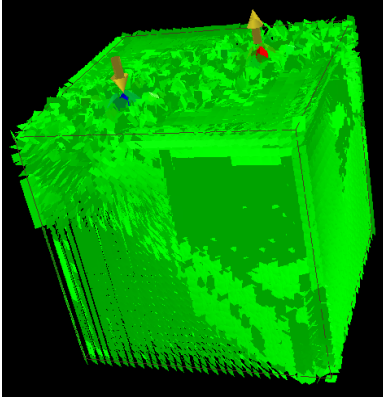


Figure 2: Double point load isotropy (linear) with arrows showing point loads

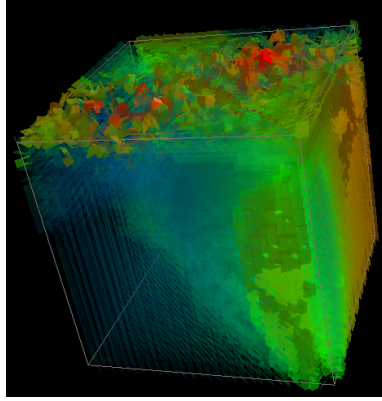


Figure 3: Opacity filtering, isotropy color and opacity (log scaled)

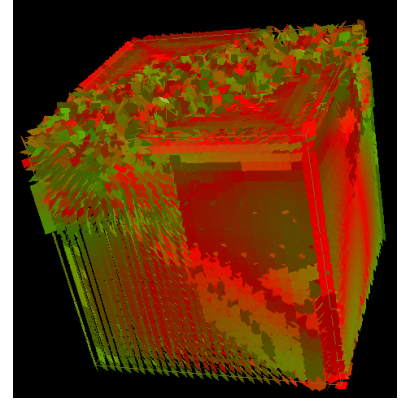


Figure 4: Double point load DC (CLVD is the dual and has the same appearance but with blue instead of red)

the data set is composed of moment tensors from acoustic emissions [8]. With thresholding, the shape of regions are also clearly delimited. Essentially, the user can create isosurface and iso-volume-like selections. The surface however, is not smooth, being composed of individually oriented planes. Finally, the application can toggle to show the *inverse* of a selected feature range, providing greater flexibility.

5.3 User Interaction

Rather than thresholding over the entire volume, a user may wish to explore from points of interest on outwards. We provide a pointer that the user can move around the volume to select various seed points. Then, on each iteration, neighboring planes get painted. This gives an animation effect of oriented planes growing out of the seed point. Thresholding constraints may also be applied, as desired. For this type of interaction, we built two data structures that save state between animation frames. One is a draw list where each entry refers to a sample point in the volume. This is initialized to all zeros to indicate no planes should be drawn; only non-zero entries have their planes drawn during an iteration. The second is a queue that holds the sample point numbers to be added to the draw list on the next iteration. In addition, the point adjacency is stored in an adjacency list, implemented as an array of linked lists. The algorithm proceeds as a simple breadth first traversal. At first glance the extra complexity may seem unnecessary; after all, for regular data we can simply use the stride of the length, width, and slice of the rectilinear sorted data. However, in many cases geomechanics data is *not* regular. Gauss points across finite elements are not lined up along X and Y. We would still like to explore a region from a selected seed point, and breadth first traversal of the mesh works well for this.

After initialization with the user's selected seed points, we take each point from the queue, add it to the draw list and check its linked list of neighbors. Here again, we depend on having neighbor connectivity available. We do a triple check before we consider adding a new point to the next iteration's queue. The sample point must meet all of the user's constraints, and neither the current draw list nor the current queue may already contain it.

The data structures and process are very similar to Gibson's Chainmail algorithm [9]. The Chainmail algorithm

enables fast deformation of volumetric objects, composed of objects such as nodes and points from Finite Element analysis. The analogy is that points and nodes move as if joined by a chainlink mesh. If a node is moved beyond a constraint, neighboring nodes will also move. Like our algorithm, on each iteration, new candidates are queued breadth-first and previously selected candidates are tested against the constraints.

6 RESULTS

We tested our application using two data sets, each of which was a single time step in a geomechanics simulation. Both data sets consisted of a field of stress tensors for geomechanical soils and solids, as described in section 4.

The first was the Boussinesq point load, where force was applied at two points on the top of the volume. The second was a bridge supported by two piles in soil. In the simulation, force was applied to one side of the bridge.

6.1 Boussinesq Point Load

Figure 2 shows isotropy in the double point load data set. Linear scaling highlights the compressive and tensile forces at the point they were applied.

The eigenvalues at these points were extremely high so the linear scale caused the rest of the volume to appear to have zero isotropy evenly throughout. However, when we change to a log scale and scale the opacity as well, the variation from cold to hot is strongly emphasized (Figure 3).

Figure 4 shows the coloring for the double couple feature. We omitted CLVD since it is calculated as the dual of DC and would appear as blue-green color mapping instead of green-red. It is clear that anisotropic regions have no correlation with isotropic regions, and combinations of constraints on several types of features may lead to better understanding of stress within a volume. For example, isotropy is largest at the point where the load is applied (Figure 2). The DC feature is strongest on the plane between the two opposite loads, a very different region of the volume (Figure 4). Positive isotropy in combination with anisotropic behavior for shear might lead to fracture.

In Figures 5 and 6, we see the results of DC thresholding. Both figures show greater than 50% similarity to the DC

feature, but the first figure has a color representing lower similarity overall. We found it interesting that using a lower threshold selected the very noisy data around the points where stress was applied. The region most closely matching a DC feature was where we expected the shear to occur – on the plane between where the two opposing forces were applied.

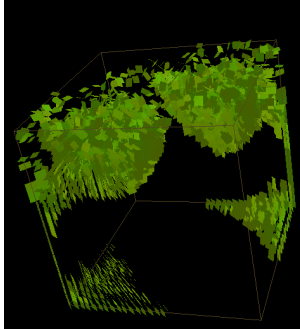


Figure 5: Double Couple thresholding, 0.50 - 0.715

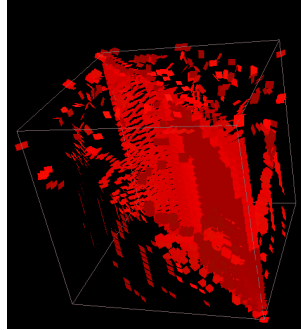


Figure 6: Double Couple thresholding, 0.975 -1.00

6.2 Bridge Pile Data Set

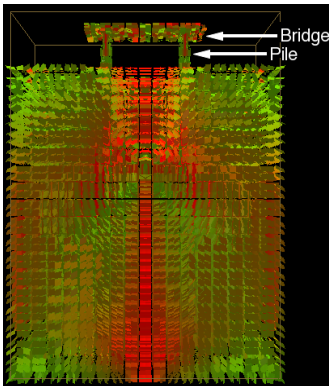


Figure 7: Bridge data set, DC coloring

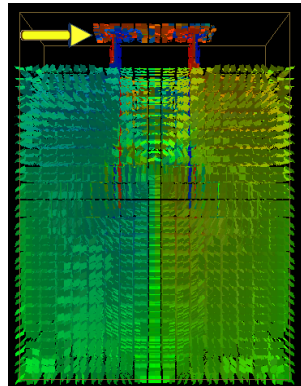


Figure 8: Eigen difference log scale coloring. Yellow arrow shows direction of applied force

Figure 7 shows the entire volume for bridge supports embedded in soil. The piles penetrate halfway down onto the soil. In the simulation, the additive stress pushed the bridge support to the left. The eigen difference coloring highlights the changes in stress with red and blue coloring above the surface and within the piles. The sharp red-blue contrast along the upper neck of the piles and in the bridge emphasizes that type of stress is flipping from linear to planar.

There is a circular appearance in the planes' orientation at the center of the volume. This is attributable to boundary effects in the simulation and represents a very important finding as it tells us that the model needs to be enlarged in order to more realistically simulate the half-space.

Figure 9 shows thresholding by isotropy. The figure is colored by log scale isotropy and shows ranges of 0.0-0.25 (negative isotropy) and 0.75-1.0 (positive isotropy). The bridge pile on the right has a color change from red to blue just

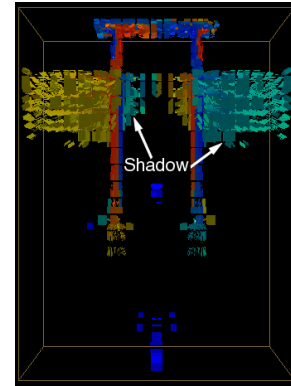


Figure 9: Bridge data set, log scaled isotropy, 0.0-0.25 and 0.75-1.0

above where the pile enters the soil, indicating that the stress has switched from positive (tension) to negative (compression). This is one of the critical features in geomechanics that can result in tensile failure. The isotropy figure also shows a shadowing effect. Shadowing comes from an analogy between the applied force and light, where a supporting member may absorb or block the force. Its shadow is an area under less stress. The shadowing is indeed interesting as it directly and visually conveys information about an important physical behavior, namely the back piles (bridge supports) will be shadowed by the front piles, and thus savings can be made in reinforcement steel for shadowed bending. It seems from the data that the isotropy (see Figure 9) also presents a visual proof that the model can and needs to be extended in the horizontal direction in order to simulate the half space more realistically. Ideally, the simulation would be sufficiently large that the boundaries would be unaffected by the applied force. This, however, is always a tradeoff with computation cost and even with this smaller model we can get meaningful results.

7 DISCUSSION AND CONCLUSION

We have explored key features from several tensor domains, looking for scalar quantities that succinctly describe geomechanical stress. We experimented using four different scalar measures and used thresholding and opacity to reduce occlusion and highlight regions of interest. Isotropy turned out to be the most useful feature among those we tried. Along with thresholding, it highlighted information about the materials' physical behavior under stress.

We also presented a new stress glyph, plane-in-a-box which provides stress orientation information and reveals trends in a volume rather well. The algorithm is cheap, providing interactive rendering rates. Our experiences with geomechanics data validate the use of the glyph to reveal interesting trends.

ACKNOWLEDGMENTS

Many thanks to Xiaoqiang Zheng for suggestions, interaction and feedback. We also thank the reviewers for their constructive critiques. This work is funded in part by a GAANN fellowship and NSF grant # ACI-9908881.

References

- [1] Keiiti Aki and Paul G. Richards. *Quantitative Seismology Theory and Methods*. W.H. Freeman and Company, 1980.
- [2] L. M. Anderson. A relative moment tensor inversion technique applied to seismicity induced by mining, 2001.
- [3] Boris Jeremić. A brief overview of neesgrid simulation platform openese: Application to the soil–foundation–structure interaction problems. In Maria Todorovska and Mehmet Chelebi, editors, *Proceedings of the Third United States–Japan Natural Resources Workshop on Soil-Structure Interaction*, Vallombrosa Center, Menlo Park, California, USA, March 29-30 2004.
- [4] Boris Jeremić and Matthias Preisig. Seismic soil–foundation–structure interaction: Numerical modeling issues. In *ASCE Structures Congress*, New York, NY, U.S.A., April 20-24 2005.
- [5] Paul D. Bourke. Intersection of a plane and a line. astronomy.swin.edu.au/~pbourke/geometry/planeline, 1991.
- [6] T. Delmarcelle and L. Hesselink. Visualizing second-order tensor fields with hyperstreamlines. *IEEE Computer Graphics and Applications*, 13(4):25–33, July 1993.
- [7] Douglas S. Dreger, Hrvoje Tkalčić, and Malcolm Johnston. Dilational processes accompanying earthquakes in the long valley caldera. *Science*, 288(5463):122–125, April 2000.
- [8] Florian Finck, Jochen H. Kurz, Christian U. Grosse, and Hans Wolf-Reinhardt. Advances in moment tensor inversion for civil engineering. In *International Symposium on Non-Destructive Testing in Civil Engineering*, 2003.
- [9] Sarah F. Gibson. 3D ChainMail: a fast algorithm for deforming volumetric objects. In Andy van Dam, editor, *Proceedings Symposium on Interactive 3D Graphics*, pages 149–154, April 1997.
- [10] Youssef M.A. Hashash, John I-Chiang Yao, and Donald C. Wotring. Glyph and hyperstreamline representation of stress and strain tensors and material constitutive response. *International Journal for Numerical and Analytical Methods In Geomechanics*, 27(7):603–626, 2003.
- [11] Boris Jeremić, Kenneth Runesson, and Stein Sture. Finite deformation analysis of geomaterials. *International Journal for Numerical and Analytical Methods in Geomechanics including International Journal for Mechanics of Cohesive–Frictional Materials*, 25(8):809–840, 2001.
- [12] Boris Jeremić, Gerik Scheuermann, Jan Frey, Zhaohui Yang, Bernd Hamann, Kenneth I. Joy, and Hans Hagen. Tensor visualizations in computational geomechanics. *International Journal for Numerical and Analytical Methods in Geomechanics*, 26:925–944, 2002.
- [13] Boris Jeremić and Christos Xenophontos. Application of the p -version of the finite element method to elasto–plasticity with localization of deformation. *Communications in Numerical Methods in Engineering*, 15:867–976, 1999.
- [14] Boris Jeremić, Christos Xenophontos, and Stein Sture. Modeling of continuous localization of deformation. In Roger Ghanem Nick Jones, editor, *Proceedings of 13th Engineering Mechanics Specialty Conference*, page 4 pages, Baltimore, Maryland, June 1999. Engineering Mechanics Division of the American Society of Civil Engineers.
- [15] Boris Jeremić, Zhaohui Yang, and Stein Sture. Influence of imperfections on constitutive behavior of geomaterials. *ASCE Journal of Engineering Mechanics*, 130(6), June 2004.
- [16] M.L. Jost and R. B. Herrmann. A student’s guide to and review of moment tensors. *Seismological Research Letters*, 60:37–57, 1989.
- [17] Gordon Kindlmann. Superquadric tensor glyph. In *Vissym’04*, pages 147–154, 2004. www.cs.utah.edu/~gk/papers/vissym04.
- [18] Gordon L. Kindlmann and David M. Weinstein. Hue-balls and lit-tensors for direct volume rendering of diffusion tensor fields. In *IEEE Visualization*, pages 183–189, 1999.
- [19] L. Knopoff and MJ Randall. Compensated linear–vector dipole–possible mechanism of deep earthquakes. *J. Geophys. Res.*, 75:4957–4963, 1970.
- [20] David Laidlaw, Eric Ahrens, David Kremers, Matthew Avallous, Russell Jacobs, and Carol Readhead. Visualizing diffusion tensor images of the mouse spinal cord. In *Proceedings of Visualization ’98*, pages 127–134, 1998.
- [21] William T. Lambe and Robert V. Whitman. *Soil Mechanics, SI Version*. John Wiley and Sons, 1979.
- [22] W. E. Lorensen and H. E. Cline. Marching cubes: A high resolution 3D surface construction algorithm. *Computer Graphics*, 21(4):163–169, 1987.
- [23] M. Ohtsu and M. Shigeishi. Three-dimensional visualization of moment tensor analysis by SiGMA-AE. *The e-Journal of Nondestructive Testing*, 7(9), September 2002. www.ndt.net/article/v07n09/02/02.htm.
- [24] Matthew O. Ward. A taxonomy of glyph placement strategies for multidimensional data visualization. In *Information Visualization*, volume 1, pages 194–210. Palgrave Macmillan, December 2002.
- [25] W.Benger and H.-C. Hege. Tensor splats. In *Visualization and Data Analysis*, pages 151–162, 2004.
- [26] C.-F. Westin, S. Peled, H. Gudbjartsson, R. Kikinis, and F. A. Jolesz. Geometrical diffusion measures for MRI from tensor basis analysis. In *ISMRM ’97*, page 1742, Vancouver Canada, April 1997.
- [27] Xiaoqiang Zheng, Beresford Parlett, and Alex Pang. Topological lines in 3D tensor fields and discriminant hessian factorization. *IEEE Transactions on Visualization and Computer Graphics*, 11(4):395–407, July/August 2005. www.cse.ucsc.edu/~pang/hessian.pdf.